BIOCHEMISTRY
including biophysical chemistry & molecular biology

Article

pubs.acs.org/biochemistry

Probing Mechanistic Similarities between Response Regulator Signaling Proteins and Haloacid Dehalogenase Phosphatases

Robert M. Immormino, Chrystal A. Starbird,† Ruth E. Silversmith, and Robert B. Bourret*

Department of Microbiology and Immunology, University of North Carolina, Chapel Hill, North Carolina 27599-7290, United States

Supporting Information

ABSTRACT: Response regulator signaling proteins and phosphatases of the haloacid dehalogenase (HAD) superfamily share strikingly similar folds, active site geometries, and reaction chemistry. Proteins from both families catalyze the transfer of a phosphoryl group from a substrate to one of their own aspartyl residues, and subsequent hydrolysis of the phosphoprotein. Notable differences include an additional Asp that functions as an acid/base catalyst and an active site well-structured prior to phosphorylation in HAD phosphatases. Both features contribute to reactions substantially faster than those for response regulators. To investigate mechanisms underlying the functional differences between response regulators and HAD phosphatases, we characterized five double mutants of the response regulator CheY designed to mimic HAD phosphatases. Each mutant contained the extra Asp paired with a phosphatase-inspired substitution to potentially position the Asp properly. Only CheY DR (Arg as the anchor) exhibited enhanced rates of both autophosphorylation with phosphoramidate and autodephosphorylation compared to those of wild-type CheY. Crystal structures of CheY DR complexed with MoO_4^{2-} or WO_4^{2-} revealed active site hydrogen bonding networks similar to those in HAD·substrate complexes, with the extra Asp positioned for direct interaction with the leaving group (phosphorylation) or nucleophile (dephosphorylation). However, CheY DR reaction kinetics did not exhibit the pH sensitivities expected for acid/base catalysis. Biochemical analysis indicated CheY DR had an enhanced propensity to adopt the active conformation without phosphorylation, but a crystal structure revealed unphosphorylated CheY DR was not locked in the active conformation. Thus, the enhanced reactivity of CheY DR reflected partial acquisition of catalytic and structural features of HAD phosphatases.

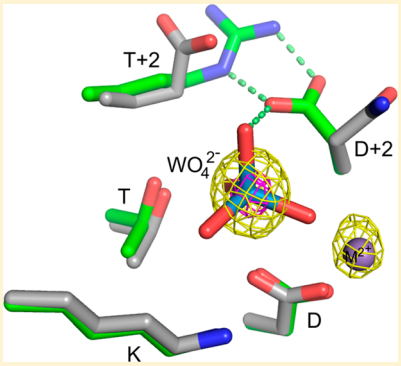

Bacteria monitor the extracellular milieu, respond to metabolic conditions, and effect virulence using two component signaling systems.[1,2] Each two-component system is minimally comprised of a histidine kinase that detects the signal and a partner response regulator that executes an output response. The response regulator acts as an allosteric molecular switch that is turned on and off by the reversible phosphorylation of an aspartyl residue. Although histidine kinases and phosphatases often regulate rates of response regulator phosphorylation and dephosphorylation *in vivo*, the response regulator receiver domain contains the conserved catalytic residues necessary and sufficient for both reactions. The ability to self-catalyze phosphoryl chemistry allows for response regulator autophosphorylation using small molecule phosphodonors, such as acetyl phosphate (AcP, $CH_3CO_2PO_3^{2-}$) or phosphoramidate (PAM, $NH_3^+PO_3^{2-}$),[3,4] as well as subsequent hydrolytic autodephosphorylation.[5] Autophosphorylation occurs via in-line nucleophilic attack by the conserved Asp (D) on the phosphorus atom of the phosphodonor, and autodephosphorylation progresses by a water molecule attacking the phosphorus within the phosphoaspartate (Figure 1B).[6] Both substitution reactions occur with inversion of stereochemistry around the phosphorus atom. The proposed transition states for both reactions are believed to be stabilized by a conserved active site that includes a bound divalent cation [coordinated by a conserved pair of acid residues (DD)], as well as threonine/serine (T) and lysine (K) residues (Figure 1A,B).

Phosphatases within the haloacid dehalogenase (HAD) superfamily share a highly similar active site and catalyze the same fundamental chemistry as response regulator receiver domains.[7−10] Like receiver domains, HAD phosphatases have a set of conserved active site residues located on the loops that follow β-strands within a domain that consists of an alternating pattern of β-strands and α-helices. Although the primary sequences of receiver domains and HAD phosphatases are related by circular permutation,[7,10] the relative locations of the conserved D, K, T, DD, and divalent cation within receivers and HAD active sites are strikingly similar (Figure 1A). Directly analogous to the autophosphorylation/autodephosphorylation reactions of response regulators, HAD phosphatases catalyze dephosphorylation of their substrates via a two-step mechanism using a phosphoaspartate enzyme intermediate that is subsequently hydrolyzed (Figure 1B).[11,12] HAD phosphatases have a broad range of natural substrates, many of which are phosphomonoesters such as phosphorylated sugars[9] and phosphoproteins.[13] Despite the similar active sites, HAD phosphatases typically exhibit rate constants ~10^2−10^4-fold greater than those of response regulators.[14] This difference highlights the different

Received: March 16, 2015
Revised: April 24, 2015
Published: April 30, 2015

DOI: 10.1021/acs.biochem.5b00286
Biochemistry 2015, 54, 3514−3527

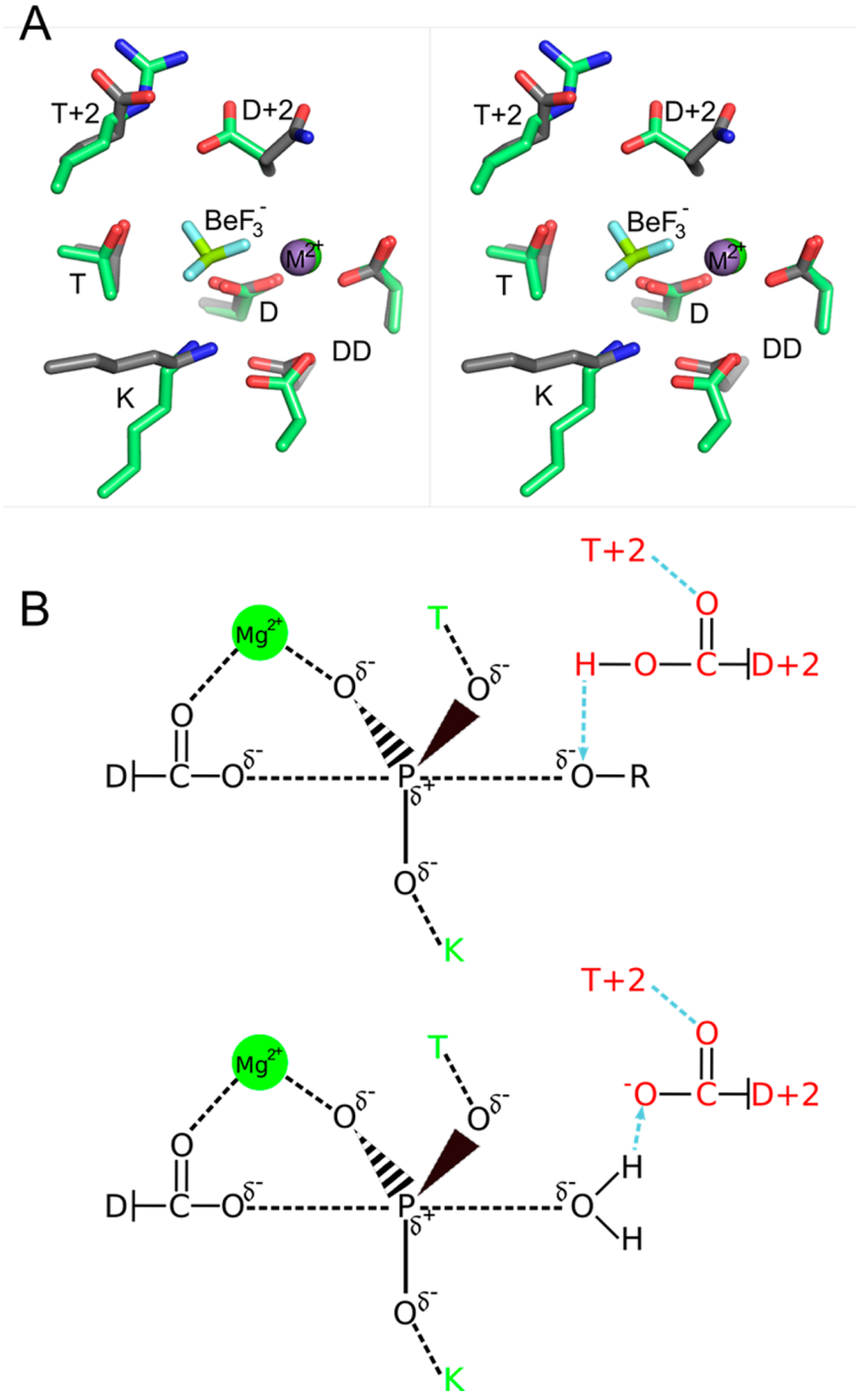

Figure 1. Similarity of active site geometries and reaction chemistry of response regulators and HAD phosphatases. (A) Stereoview of superimposed active sites of *Escherichia coli* CheY (gray sticks, PDB entry 1FQW) and *Bacteroides thetaiotaomicron* VPI-5482 hexose phosphate phosphatase (HPP) (green sticks, PDB entry 2RBK). The divalent cations are shown as purple (CheY) or green (HPP) spheres. The BeF_3^- ion shown is present in the CheY structure. The VO_4^{2-} that occupies the same location in HPP is not shown for the sake of clarity. D, DD, T, and K are defined in the text and are conserved in both families. Additionally, the residue at position D + 2 is conserved as an Asp in HAD phosphatases. (B) Proposed trigonal bipyramidal transition states (black) for the phosphorylation (top) and dephosphorylation (bottom) substitution reactions of response regulators and HAD phosphatases. Conserved active site features involved in transition state stabilization that are shared by response regulators and HAD phosphatases (T, K, and Mg^{2+}) are colored green. In addition, HAD phosphatases contain a conserved Asp at position D + 2 (red) that acts sequentially as an acid (top) and base (bottom) catalyst and is anchored by the residue at position T + 2 (red).

roles for the phosphorylated intermediate in the two families. HAD phosphatases evolved to catalyze dephosphorylation and typically only briefly exist as phosphorylated enzyme intermediates. In contrast, response regulators must persist in the phosphorylated (activated) form to facilitate signal transduction and have dephosphorylation kinetics on the time scale of the processes they regulate.[15]

Two features of HAD phosphatases that likely contribute to their faster kinetics are an additional conserved Asp residue positioned two residues C-terminal to the site of phosphorylation

DOI: 10.1021/acs.biochem.5b00286
Biochemistry 2015, 54, 3514−3527

(position D + 2) and an active site so well structured to stabilize the transition state to be capable of distorting the shape of substrate analogues.[11] The additional Asp acts alternately as a catalytic acid and base in the two phosphatase half-reactions[16−18] (Figure 1B) and is often anchored in position by a semiconserved residue (often an Arg, Lys, Thr, Trp, or Tyr) at position T + 2 (two residues C-terminal to the conserved Ser/Thr), which helps to maintain the active site structure.[11] In contrast, position D + 2 is rarely an Asp in response regulators, accounting for <2% of response regulator sequences in a survey (R. M. Immormino and R. B. Bourret, unpublished observations) of ∼14000 sequences from the MiST2.1[19] database. In addition, response regulators are dynamic proteins that exhibit modest but functionally important conformational changes at the active site and allosterically linked surfaces. Residue T + 2 lies on a particularly mobile loop.[20,21] Despite these differences with HAD phosphatases, the residues at positions D + 2 and T + 2 in response regulators have been identified as playing roles in modulation of both autophosphorylation and autodephosphorylation reactions.[15,22,23] Furthermore, the D + 2 and T + 2 residues interact with each other in multiple X-ray crystal structures of response regulator receiver domains.[15,24]

To more fully understand the mechanistic similarities and differences between response regulators and HAD phosphatases, we explored the effect of placing an Asp at position D + 2 and a partner residue at position T + 2 in the response regulator *Escherichia coli* CheY. CheY consists only of a receiver domain and has been used extensively as a model system to elucidate kinetic determinants that modulate receiver domain phosphotransfer reactions[22,23] as well as the allosteric conformational changes linked to phosphorylation.[21,25] Of a set of five CheY double mutants designed to mimic the HAD active site, CheY DR (an Asp at position D + 2 and an Arg at position T + 2) uniquely exhibited enhanced rate constants for both autophosphorylation and autodephosphorylation. Structural and biochemical analysis indicated that the enhanced kinetics of CheY DR could be explained by partial acquisition of some properties of HAD phosphatases. Crystal structures of CheY DR complexed with MoO_4^{2-} or WO_4^{2-} revealed a CheY backbone in a fully activated conformation and an active site hydrogen bonding network between Asp at position D + 2 and the Arg at position T + 2 that positioned the Asp to interact with the leaving group atom of the phosphodonor (for autophosphorylation) or the attacking water molecule (for autodephosphorylation). However, pH profiles of autocatalytic rate constants did not indicate an altered pK_a for the Asp at position D + 2 as would be predicted for function as a true acid/base catalyst. CheY DR also exhibited an enhanced binding affinity for the target peptide $FliM_{1-16}$ relative to that of wild-type CheY, suggesting that a shift toward an activated (i.e., phosphorylated/FliM binding) global conformation provided a more complete active site mold as exhibited by HAD phosphatases.

EXPERIMENTAL PROCEDURES

Site-Directed Mutagenesis and Protein Purification. Genes encoding the CheY variants [termed CheY (D + 2)(T + 2), i.e., CheY DR, CheY DK, CheY DY, CheY DQ, and CheY DT] were generated by QuikChange mutagenesis (Agilent Technologies) of pKC1,[26] a pET28a-derived vector encoding wild-type *E. coli* CheY with an N-terminal thrombin-cleavable hexahistidine tag. The substitutions at position T + 2 were chosen on the basis of anchoring residues (Arg, Lys, Thr, Trp, and Tyr) found in HAD phosphatase structures.[11] A Trp substitution at position T + 2 was not constructed because our assays of reaction kinetics depend on the fluorescence of the unique Trp present at position D + 1 in wild-type CheY. A Gln substitution at position T + 2 was tested because its size and chemical properties were potentially compatible with anchoring the Asp at position D + 2. After thrombin cleavage, an extra GlySerHis was present at the CheY N-terminus, which does not affect CheY autophosphorylation[26] or autodephosphorylation[27] kinetics. Variation at the N-terminus is not known to affect the structure of the active site, located on the opposite side of the receiver domain. Overexpression of the CheY DX variants was performed with BL21(DE3) cells containing the appropriate pKC1 plasmid. Briefly, 1 L of lysogeny broth containing 30 μg/mL kanamycin was inoculated with 15 mL of overnight culture and grown to an OD_{600} of 1.0. The culture was then induced with 1 mM isopropyl β-D-1-thiogalactopyranoside at room temperature overnight. Cell lysates [in 50 mM NaH_2PO_4 (pH 8.0), 300 mM NaCl, and 10 mM imidazole] were purified by Ni-NTA agarose (Qiagen) chromatography. The eluted protein [in 50 mM NaH_2PO_4 (pH 8.0), 300 mM NaCl, and 150 mM imidazole] was incubated with human α-thrombin (Hemolytic Technologies Inc.) at a 1:6000 (w/w; thrombin:CheY) ratio overnight at room temperature. A final purification step to separate CheY from thrombin and the cleaved tag was gel filtration (Superdex75 16/60, GE) in TMG buffer [25 mM Tris (pH 7.5), 5 mM $MgCl_2$, and 10% (v/v) glycerol]. Wild-type CheY and the T + 2 single mutants (CheY NK, NR, NA, NY, and NQ) were expressed and purified as previously described.[28] Briefly, K0641*recA* containing pRS3[29] or mutant plasmids were grown to an OD_{600} of 1.0 and induced with 100 μg/mL β-indole acrylic acid at 37 °C overnight. Cell lysates in TMG buffer were purified by dye affinity chromatography (Affigel-Blue, Bio-Rad) followed by size-exclusion chromatography (Superdex 75, GE Healthcare). Concentrations for all purified CheY preparations were determined spectrophotometrically using an extinction coefficient at 280 nm of 0.727 M^{-1} cm^{-1}.[4]

Fluorescence Measurement of CheY Autophosphorylation and Autodephosphorylation Kinetics. With the exception of CheY DR and CheY DK autophosphorylation reactions, autophosphorylation and autodephosphorylation time courses were measured by continuous monitoring of CheY intrinsic tryptophan fluorescence on a PerkinElmer LS-50B spectrofluorimeter with an Applied Photophysics (Surrey, U.K.) RX2000 rapid mixer accessory (dead time of 8 ms) and PerkinElmer FL WINLAB V3 software as previously described.[23,30] The kinetics of CheY DR and CheY DK autophosphorylation were too fast to be measured using the LS-50B instrument, so measurements were taken using a Jobin Yvon FluoroLog 322 spectrofluorimeter (response time of 3 ms) equipped with a F-3009 μFlow stopped-flow apparatus (dead time of <5 ms) and associated DATAMAX Version 2 software at the University of North Carolina Macromolecular Interactions Facility. In each case, the excitation and emission wavelengths were set to 295 and 346 nm, respectively, and samples were maintained at a constant temperature of 25 °C with a circulating water bath. Data points were recorded at 20 ms intervals on the LS-50B instrument and 10 ms intervals on the FluorLog 322 instrument.

For autophosphorylation experiments, equal volumes of 10 μM CheY and varying concentrations of phosphodonor, each in 100 mM HEPES (pH 7.0) and 10 mM $MgCl_2$, were mixed. The phosphodonor was either phosphoramidate (PAM) with four final reaction concentrations ranging from 0.5 to 30 mM or acetyl phosphate (AcP) with four final reaction

DOI: 10.1021/acs.biochem.5b00286
Biochemistry 2015, 54, 3514−3527

concentrations ranging from 10 to 50 mM. Because ionic strength affects CheY autophosphorylation kinetics,[31,32] KCl was added to the phosphodonor solution to maintain a constant ionic strength of 300 mM (phosphodonor with KCl). Time courses monitoring the accumulation of CheY-P were fit to a single-exponential decay model to determine k_{obs}. The data were further analyzed on the basis of the following reaction scheme[3,32] (illustrated with PAM as a phosphodonor)

Scheme 1

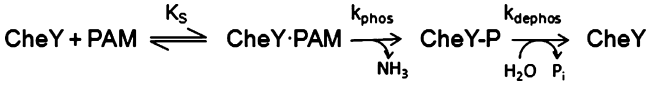

where K_S is the equilibrium dissociation constant for formation of the noncovalent complex between CheY and PAM, k_{phos} is the rate constant for phosphotransfer within the complex, and k_{dephos} is the autodephosphorylation rate constant. k_{obs} is a function of the kinetic parameters from Scheme 1 as follows:[32]

$$k_{obs} = (k_{phos}/K_S)[PAM] + k_{dephos} \quad (1)$$

For each CheY variant, k_{obs} was measured at four different phosphodonor concentrations. Plots of k_{obs} versus phosphodonor concentration were linear in all cases, and the slope gave the apparent bimolecular rate constant, k_{phos}/K_S.

Rate constants for CheY autodephosphorylation were determined using the pH jump method.[27,32] Mutant or wild-type CheY [10 μM in 10 mM HEPES (pH 7.0) and 20 mM $MgCl_2$] was phosphorylated with PAM at ~5 times the concentration of PAM required to phosphorylate half of the CheY at steady state. The sample was then mixed using the rapid mixing accessory with an equal volume of pH jump buffer [200 mM sodium carbonate (pH 10.2)], which drastically retards the phosphorylation reaction, so that the observed time course for the increase in fluorescence reflects the dephosphorylation reaction alone. Each time course was fit to a single-exponential decay to determine the first-order rate constant, k_{dephos}. CheY autodephosphorylation rate constants determined by the pH jump method and by loss of radioactive phosphoryl groups agree within a factor of <2.[27]

Rapid Dilution Assay To Determine the pH Dependence of Autodephosphorylation. The effect of pH on autodephosphorylation was tested with a rapid dilution assay. To isolate the dephosphorylation reaction, 100 μM CheY in autophosphorylation buffer was first phosphorylated with PAM (50 mM for wild-type CheY or 5 mM for CheY DR and CheY DY) in a 15 μL reaction volume. The reaction mixture was then diluted 100-fold with 10 mM $MgCl_2$ and one of the following buffers at 100 mM: sodium carbonate (pH 10.2), Tris (pH 8.9), Tris (pH 8.0), HEPES (pH 7.0), MES (pH 6.5), sodium cacodylate (pH 5.9), sodium citrate (pH 5), or sodium acetate (pH 4.5). Phosphorylation and dilution were performed in a 1.5 mL quartz fluorescence cuvette while Trp fluorescence was being monitored. The observed pseudo-first-order rate of autophosphorylation is proportional to the concentration of phosphodonor and thus is reduced by 2 orders of magnitude upon dilution. The observed change in fluorescence for these experiments (k_{obs}, eq 1) following dilution is dominated by the k_{dephos} term.

Autophosphorylation pH Profiles. The pH dependence of autophosphorylation was measured using a variation of the autophosphorylation assay described above. Briefly, equal volumes of 10 μM CheY and a phosphodonor solution of 5 mM PAM and 95 mM KCl were mixed using the rapid mixer accessory. Both CheY and phosphodonor were suspended in the set of pH buffers consisting of 10 mM $MgCl_2$ and 100 mM buffer as described for the rapid dilution assay. The observed rate constant (k_{obs}, eq 1) reflects contributions from both rate constants for autophosphorylation (k_{phos}/K_S) and autodephosphorylation (k_{dephos}). To separate the effect of pH on k_{phos}/K_S, the k_{dephos} value determined using the pH jump method was subtracted from k_{obs} giving eq 2. To more readily compare the CheY mutants, $k_{obs} - k_{dephos}$ was normalized to the value at pH 6.5 giving eq 3.

$$k_{obs} - k_{dephos} = (k_{phos}/K_S)[PAM] \quad (2)$$

$$\frac{k_{obs} - k_{dephos}}{(k_{obs} - k_{dephos})_{pH6.5}} = \frac{(k_{phos}/K_S)}{(k_{phos}/K_S)_{pH6.5}} \quad (3)$$

Enzyme Activity toward *p*-Nitrophenyl Phosphate. Wild-type CheY or CheY DR (18.4 μM) was added to 200 mM *p*-nitrophenyl phosphate (pNPP, Sigma) in a 1.0 mL cuvette and the optical density at 450 nm read continuously to monitor the release of *p*-nitrophenolate. The buffers (present at 100 mM) were sodium salts of HEPES (pH 7.0), cacodylate (pH 6.5), citrate (pH 5.0), or acetate (pH 4.5). All buffers contained 10 mM $MgCl_2$. The positive controls were the HAD phosphatase *E. coli* YbiV[33] and calf intestinal phosphatase.

Fluorescence Measurement of Binding between CheY and $FliM_{1-16}$. Binding affinities between the peptide MGDSILSQAEIDALLN, which corresponds to the 16 amino-terminal residues of *E. coli* FliM ($FliM_{1-16}$), and CheY were measured using tryptophan fluorescence as previously described.[34,35] $FliM_{1-16}$ (final concentrations of 10−1000 μM) was titrated into 5 μM CheY in autodephosphorylation buffer [10 mM HEPES (pH 7.0) and 20 mM $MgCl_2$], and the resulting fluorescence quench was monitored. The measured intensities were corrected for dilution, and K_d values were determined using Prism (GraphPad) to fit the data to a one-site binding model.

Crystallization, Data Collection, Structure Solution, and Refinement. Crystals of CheY DX mutants were grown by hanging drop vapor diffusion at room temperature. Crystals of the CheY·BeF_3^-·Mn^{2+} complexes were obtained by adding 20 mM $MnCl_2$, 1 mM $BeCl_2$, and 10 mM NaF to the CheY variants (at 4.3−8.9 mg/mL) prior to crystallization. Diffraction quality crystals were found under conditions[36] ranging from 1.6 to 2.4 M ammonium sulfate, 5% (v/v) glycerol, 100 mM Tris, and pH 7.5−8.25 with a 1:1 protein:reservoir buffer drop ratio. Crystals of the CheY variants in the absence of BeF_3^- were obtained using 120−160 mM calcium acetate, 100 mM sodium cacodylate (pH 6.0), 20 mM $MnCl_2$, and 28−31% (v/v) PEG8000 as the reservoir solution with a 1:1 drop ratio.[37] Crystals generally grew overnight or over the course of <1 week in various forms. For conditions with BeF_3^-, the main crystal type was rhombic bipyramidal, but several of the CheY variants also formed rod-shaped crystals, which tended to diffract better.

CheY·BeF_3^-·Mn^{2+} and CheY·Mn^{2+} crystals were cryoprotected with glycerol as previously described,[15] or by serial transfers through buffers with increasing amounts of glycerol. Cryoprotected crystals were flash-cooled in liquid nitrogen in preparation for data collection. X-ray diffraction images were collected at SERCAT beamlines 22-BM and 22-ID at APS.

DOI: 10.1021/acs.biochem.5b00286
Biochemistry 2015, 54, 3514−3527

Table 1. Autophosphorylation and Autodephosphorylation Rate Constants of CheY Variants

CheY designation[a]	amino acid		k_{phos}/K_S (M^{-1} s^{-1})[b]		k_{dephos} (min^{-1})[c]
	position D + 2	position T + 2	phosphoramidate	acetyl phosphate	
DX Set (HAD mimics)					
DR	D	R	820 ± 26	3.9 ± 0.4	20 ± 1.7
DK	D	K	170 ± 3	5.7 ± 0.5	2.8 ± 0.06
DQ	D	Q	13 ± 0.2	1.5 ± 0.05	4.8 ± 0.03
DY	D	Y	130 ± 10	0.5 ± 0.05	0.7 ± 0.05
DT	D	T	4.1 ± 0.05	0.3 ± 0.1	1.7 ± 0.02
DE	D	E	3.7 ± 0.55[d]	<0.2[d]	5.5 ± 0.4[e]
NX Set					
NR	N	R	93 ± 18[d]	62 ± 5.5[d]	0.69 ± 0.04[e]
NK	N	K	60 ± 7.3[d]	42 ± 0.9[d]	1.2 ± 0.3[e]
NQ	N	Q	19 ± 3[d]	36 ± 1.8[d]	3.9[f]
NY	N	Y	240 ± 34[d]	13 ± 1.9[d]	0.26 ± 0.01[e]
NA	N	A	10 ± 0.8[d]	18 ± 2.0[d]	1.5[f]
wild type	N	E	9.2 ± 0.9	10 ± 0.7	3.2 ± 0.2

[a]CheY variants are mentioned in the text by "CheY" followed by the single-letter codes for the amino acids at positions D + 2 and T + 2 (CheY residues 59 and 89, respectively). [b]Mean and standard deviation of autophosphorylation rate constants (n = 3). See Experimental Procedures or footnote [d] where indicated. [c]Mean and standard deviation of autodephosphorylation rate constants (n = 3). See Experimental Procedures or footnote [e] or [f] where indicated. [d]From ref 23. [e]From ref 22. [f]From ref 79.

Diffraction data were reduced and scaled using HKL2000[38] or XDS.[39]

Structures were also obtained for CheY DR bound to MoO_4^{2-} or WO_4^{2-}. The crystals were grown from conditions similar to those used for the CheY·BeF_3^-·Mn^{2+} complexes [2.45−2.6 M ammonium sulfate, 5% (v/v) glycerol, and 100 mM Tris (pH 7.5)]. Prior to crystallization drops being set up, 20 mM $MnCl_2$ and either 2 mM ammonium molybdate or 10 mM sodium tungstate were added to CheY DR, and the mixture was incubated for 10 min. Single anomalous dispersion (SAD) data were collected at the LI absorption edge of tungsten (1.02631 Å) to 2.1 Å resolution for both complexes (Table 2). At this wavelength, tungsten, molybdenum, and manganese have anomalous signals of 12.2, 1.3, and 1.4 e^{-1}, respectively,[40] allowing for confident distinction of molybdate and tungstate from sulfate ions (0.25 e^{-1}) present at up to 2.6 M in the crystallization buffer.

Initial phases for the CheY crystals were obtained by molecular replacement using PDB entry 1FQW[41] (CheY·BeF_3^-·Mg^{2+} with CheY in the activated conformation) or 3CHY[42] (apo-CheY with CheY in an unactivated conformation) as the search models. Initial models were improved by iterative rounds of model building in Coot[43] and structure refinement with PHENIX.[44] Prior to deposition, the models were validated using MolProbity.[45] Tables 2 and 3 and Table S1 of the Supporting Information contain summaries of diffraction data and refinement statistics. For structural comparisons, Cα rmsd (root-mean-square deviation) values were determined using the align command in PyMOL (PyMOL Molecular Graphics System, version 1.4, Schrödinger, LLC).

RESULTS

A CheY HAD Mimic Exhibited Enhanced Rates of Autophosphorylation and Autodephosphorylation. The faster reaction kinetics observed for HAD phosphatases relative to those of response regulators are due in part to an additional conserved active site Asp at position D + 2 [two residues from the phosphorylatable Asp (D)]. The Asp at position D + 2 is often held in place via hydrogen bonding or salt bridge interactions with a residue at position T + 2,[11] thus orienting the Asp side chain for direct interaction with the leaving group (during formation of the Asp−P intermediate) or with the water oxygen (during hydrolysis of the Asp−P intermediate) (Figure 1B). To assess the impact of the presence of an Asp at position D + 2 in response regulators with various potential anchoring residues at position T + 2, we constructed a set of five CheY DX proteins where D represents the substitution of an Asp at position D + 2 (Asn59 in wild-type CheY) and X is the substitution of either Arg, Gln, Lys, Thr, or Tyr, at position T + 2 (Glu89 in wild-type CheY). For CheY, the two steps that correspond to the HAD phosphatase half-reactions (autophosphorylation and autodephosphorylation, respectively) can be monitored independently and with high precision using stopped-flow fluorescence and by exploiting the difference in tryptophan emission for phosphorylated and unphosphorylated CheY.

Measured bimolecular rate constants (k_{phos}/K_s) for autophosphorylation of CheY DX double mutants with the phosphodonors acetyl phosphate (AcP) and phosphoramidate (PAM) as well as autodephosphorylation rate constants (k_{dephos}) are listed in Table 1. Because the goal of this study was to assess the extent to which the CheY scaffold can kinetically and mechanistically mimic an HAD phosphatase by utilizing an aspartate at position D + 2 as an additional catalytic residue, the rate constants were compared to those of the analogous CheY single mutants with an Asn (the wild-type residue) at position D + 2 and the same residue at position T + 2, reported in a previous study.[23] For autophosphorylation with AcP, the five CheY DX variants for which comparison was possible gave reduced rate constants (between ∼7- and 26-fold) relative to that of the matched CheY NX single mutant, indicating that the Asp at position D + 2 actually had detrimental effects on kinetics, the opposite of the expected result for successful mimicry of catalysis by HAD phosphatases. This result is consistent with the previously observed deleterious effect of net negative charge of position D + 2/T + 2 side chains for CheY autophosphorylation with AcP,[23] which likely masked any potential specific catalytic function of the Asp at position D + 2.

In contrast to the AcP results, there was significant variation in the rate constants for the CheY DX variants relative to those of the CheY NX mutants for autophosphorylation with PAM (Table 1). We previously found that rate constant variation for

DOI: 10.1021/acs.biochem.5b00286
Biochemistry 2015, 54, 3514−3527

CheY autophosphorylation with zwitterionic PAM correlates with the nonpolar surface area of position D + 2/T + 2 side chains[23] and the rate constants for the CheY NX set largely reflect these differences. Three of the five CheY HAD mimics (CheY DY, DQ, and DK) gave PAM autophosphorylation rate constants that were within 3-fold of that of the corresponding CheY NX variant, indicating that the Asp at position D + 2 functioned like the Asn. CheY DT exhibited an autophosphorylation rate constant for PAM that was less than that of any measured CheY NX protein,[23] again suggesting no special contribution from the Asp at position D + 2. The CheY NT mutant was not available for direct comparison, and CheY DT was not characterized further. CheY DR, however, exhibited a PAM autophosphorylation rate constant that was ~9-fold greater than that of CheY NR (and ~90-fold greater than that of wild-type CheY), suggesting that the negative charge of the Asp at position D + 2 functioned in catalysis. Furthermore, CheY DR was also the only CheY DX variant with a substantially enhanced autodephosphorylation rate constant. Whereas CheY DY, DQ, and DK all gave autodephosphorylation rate constants within ~3-fold of that of the CheY NX analogue, CheY DR gave an autodephosphorylation rate constant ~30 times that of CheY NR (and ~6-fold greater than that of wild-type CheY). Thus, CheY DR is the most probable candidate for a CheY HAD mimic in which the Asp at position D + 2 plays a catalytic role that is dependent on the acidic side chain.

Accelerated Reaction Rates for CheY DR Are Not Due to Acid/Base Catalysis. One possible mechanism to account for the accelerated reaction rates for both CheY DR autophosphorylation with PAM and autodephosphorylation (Table 1) could be that the Asp at position D + 2 acts as an acid/base catalyst, as in the HAD phosphatases (Figure 1B). Acidic residues (Asp or Glu) that act as acid/base catalysts typically have pK_a values near neutral,[46] so that appreciable amounts of the protonated and unprotonated forms are present. If the Asp at position D + 2 in CheY DR acts as a catalytic base in autodephosphorylation, then pH profiles for CheY DR autodephosphorylation might be expected to exhibit a transition toward lower rate constants in the mildly acidic pH range, in contrast to that of wild-type CheY, for which autodephosphorylation rate constants are essentially independent of pH over a broad pH range.[4] However, the autodephosphorylation rate constants for CheY DR, CheY DY, and wild-type CheY were essentially constant over a wide pH range (4.5−10.2) (Figure 2A). Thus, none of the three tested CheY variants contain a residue with a pK_a above ~4.5 that contributes to catalysis in its deprotonated state, as would be expected for a base catalyst.

We also considered the possibility that acid catalysis could account for the accelerated rate of CheY DR autophosphorylation with PAM (Table 1). However, at pH 7.0 (the pH at which the rate constant was measured), PAM exists as a zwitterion with a protonated nitrogen (+1) and two oxygen monoanions (−2). Thus, for PAM, the proton is already present on the leaving group atom and acid catalysis by the enzyme is not required. PAM loses the nitrogen proton with a pK_a of ~8.0, and wild-type CheY reacts with PAM only under pH conditions where the nitrogen is protonated.[4] We investigated the possibility that CheY DR autophosphorylation may exhibit a pH range broader than that of wild-type CheY, which could reflect acid catalysis by a residue with a pK_a above ~7. However, the normalized pH dependencies of PAM autophosphorylation for wild-type CheY and CheY DR [as well as CheY DK, DY, and DQ (Figure 2B)] were virtually superimposable despite large differences in absolute rates. All of the pH profiles had a transition that correlated with the pK_a of PAM,[47] thus giving no positive evidence of acid catalysis by CheY DR.

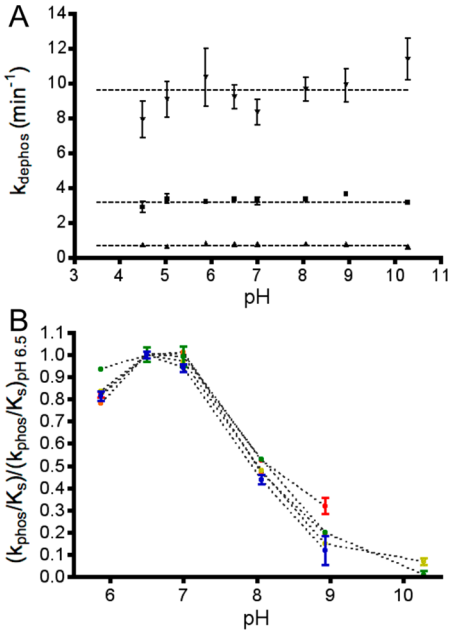

Figure 2. pH sensitivities of autodephosphorylation and autophosphorylation rate constants. (A) Autodephosphorylation rate constants (mean and standard deviation; $n \geq 3$) plotted for wild-type CheY at 25 °C (■), CheY DY at 25 °C (▲), and CheY DR at 15 °C (▼). The rate constants were measured with fluorescence using the rapid dilution method. Horizontal lines indicate the autodephosphorylation rate constants measured by the pH jump method (pH 10.2). (B) Rate constants (mean and standard deviation; $n \geq 3$) for autophosphorylation with PAM normalized to the rate at pH 6.5 for wild-type CheY (red), CheY DR (green), CheY DK (orange), CheY DY (yellow), and CheY DQ (blue).

Finally, we tested the ability of CheY DR to hydrolyze *p*-nitrophenyl phosphate (*p*NPP). Many HAD phosphatases readily react with *p*NPP,[14] a phosphomonoester whose rate of hydrolysis would be expected to benefit greatly from acid catalysis. However, CheY DR exhibited no detectable reactivity toward *p*NPP over the pH range of 4.5−7.5 (data not shown). Although this is a negative result, taken together with the pH profile results (Figure 2), we conclude that it is unlikely that the Asp at position D + 2 in CheY DR acted as a true acid/base catalyst in the phosphorylation and dephosphorylation reactions.

Structures of CheY DR Complexed with WO_4^{2-} or MoO_4^{2-}. Without evidence of acid/base catalysis, structural analysis was used to gain insight into the mechanism by which CheY DR uniquely enhanced rates of both CheY autophosphorylation and autodephosphorylation. We obtained high-quality crystals of CheY DR complexed with Mn^{2+} and the phosphate analogues molybdate (MoO_4^{2-}) or tungstate (WO_4^{2-}). The CheY DR·MoO_4^{2-}·Mn^{2+} and CheY DR·WO_4^{2-}·Mn^{2+} structures, both determined to 2.1 Å resolution (Table 2), represent the first structures of which we are aware of receiver domains complexed with these ions. The presence of MoO_4^{2-} or WO_4^{2-} was confirmed by calculation of anomalous difference Fourier maps using phases calculated from the molecular replacement solution. As seen in Figure 3 and Figure S1 of the Supporting Information, the >4σ peak for molybdenum and a >15σ peak for tungsten indicate that the ions are bound at the active site.

DOI: 10.1021/acs.biochem.5b00286
Biochemistry 2015, 54, 3514−3527

Table 2. Summary of Data Collection and Refinement Statistics for CheY DR Complexed with MoO_4^{2-} or WO_4^{2-}

	CheY DR·MoO_4^{2-}·Mn^{2+}	CheY DR·WO_4^{2-}·Mn^{2+}
	Diffraction Data	
PDB entry	3RVR	3RVS
source	APS 22-BM	APS 22-BM
space group	$P2_12_12_1$	$P2_12_12_1$
a, b, c (Å)	53.51, 53.63, 161.84	53.56, 53.62, 162.82
α, β, γ (deg)	90, 90, 90	90, 90, 90
wavelength (Å)	1.02631	1.02631
resolution (last shell) (Å)[a]	50−2.10 (2.15−2.10)	50−2.10 (2.15−2.10)
no. of unique reflections	27965	52812
completeness (last shell) (%)	99.8 (100)	99.9 (100)
average I/σ_I (last shell)	20.2 (5.3)	15.3 (4.3)
redundancy (last shell)	7.0 (6.7)	11.2 (11.4)
R_{sym}[b] (last shell) (%)	7.2 (38.4)	11.3 (60.3)
	Refinement	
refinement package	PHENIX 1.7_650	PHENIX 1.7_650
resolution range (Å)	19.73−2.10	19.31−2.10
no. of reflections	27715	52807
no. of nonsolvent atoms[c]	1995	1986
no. of solvent atoms and heteroatoms[c]	385	378
no. of molecules in the asymmetric unit	2	2
rmsd from ideality		
bond lengths (Å)	0.011	0.010
bond angles (deg)	1.288	1.328
R value[d] (%)	17.1	14.8
R_{free}[d] (%)	18.8	18.4

[a]Resolution limit defined as the highest-resolution shell where the average I/σ_I was >2. [b]$R_{merge} = \sum_{hkl}\sum_i|I_{i(hkl)} - \langle I_{(hkl)}\rangle|/\sum_{hkl}\sum_i I_{i(hkl)}$. [c]Non-hydrogen atoms and alternate atoms are counted once. [d]$R = \sum|F_o - F_c|/\sum F_o$; ∼5% of reflections were used to calculate R_{free}.

The CheY DR cocrystal structures were analyzed for both global backbone conformation and details of the active site. Like all receiver domains, CheY is an allosteric protein and exhibits both "unactivated" and "activated" global conformations for signal transduction, with the activated signaling conformation dominating in the phosphorylated state. The conserved differences between unactivated and activated receiver domain conformations are evident in comparison of structures of the unphosphorylated domain with structures of models of the phosphorylated protein, most often using the phosphoryl analogue BeF_3^-.[41] The phosphoprotein intermediate is generally too labile to isolate in crystals. In both the MoO_4^{2-} and WO_4^{2-} structures, the CheY backbone and relevant side chains displayed all the hallmarks of a fully activated receiver domain, including rotameric switching of residues Y106 and T87 and an ∼4 Å shift of the $\beta4\alpha4$ loop. The global similarity (Figure 3A) was reflected in Cα rmsd values of 0.182 and 0.217 Å in comparison of CheY·BeF_3^-·Mn^{2+} (PDB entry 1FQW) to CheY DR·MoO_4^{2-}·Mn^{2+} and CheY DR·WO_4^{2-}·Mn^{2+}, respectively. In contrast, the Cα rmsd values for comparison of CheY DR·MoO_4^{2-}·Mn^{2+}, CheY DR·WO_4^{2-}·Mn^{2+}, and CheY·BeF_3^-·Mn^{2+} to the unactive CheY·Mg^{2+} structure (PDB entry 2CHE) were 0.874, 0.882, and 0.841 Å, respectively.

Close-up views of the active sites show that both the MoO_4^{2-} and WO_4^{2-} anions retained an essentially tetrahedral geometry (Figure 3 and Figure S1 of the Supporting Information for $2F_o - F_c$ density maps). In both structures, three of the four oxygen atoms from the anion essentially overlay positions

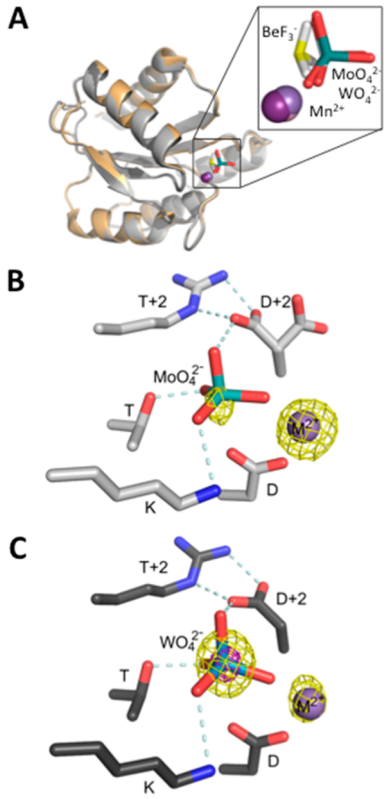

Figure 3. X-ray crystal structures of CheY DR with bound MoO_4^{2-} or WO_4^{2-}. (A) Overlay of CheY DR·MoO_4^{2-}·Mn^{2+} (light gray ribbon), CheY DR·WO_4^{2-}·Mn^{2+} (dark gray ribbon), and wild-type CheY·BeF_3^-·Mn^{2+} (PDB entry 1FQW, orange ribbon). Mn^{2+} ions are represented with purple spheres, and the MoO_4^{2-}, WO_4^{2-}, or BeF_3^- ions are shown as sticks with Mo and W (teal), Be (yellow), and F (white). The inset is a close-up of the active site ligands. (B and C) Close-up of the active sites of CheY DR·MoO_4^{2-}·Mn^{2+} and CheY DR·WO_4^{2-}·Mn^{2+}, respectively, using the same coloring as in panel A. In both structures, the Asp at position D + 2 is oriented to form a divalent salt bridge with the Arg at position T + 2. Additionally, the Asp at position D + 2 forms a hydrogen bond with the apical oxygen of the bound molybdate or tungstate. In panel B, the anomalous difference Fourier map (yellow mesh) is contoured at 4σ and has peaks that roughly correspond with the positions of the Mn and Mo atoms. Similarly, in panel C, peaks are observed at 5σ (yellow mesh) for Mn and W and additionally at 15σ (magenta mesh) for W. The relative peak heights and atom identities for the anomalous scattering atoms are consistent with expectations for the X-ray wavelength used [LI absorption edge of tungsten (1.02631 Å)]. Hydrogen bonding and electrostatic interactions are represented by light blue dashed lines, and Mn^{2+} is represented as a purple sphere.

occupied by the three fluorine atoms in structures of CheY·BeF_3^-·Mn^{2+} (Figure 3A, inset) and the three oxygen atoms make interactions with protein atoms identical to those of the fluorines in the BeF_3^- structure. However, the stereochemistry of MoO_4^{2-} or WO_4^{2-} is inverted relative to that of BeF_3^-, with the fourth oxygen atom projecting out toward solvent (Figure 3A, inset). This arrangement suggests that these structures are models of binding of the substrate to CheY prior to phosphorylation or models of the dephosphorylated protein before dissociation of the phosphate product. In this context, the fourth oxygen atom would be in the location of the leaving group atom during autophosphorylation or the water oxygen during autodephosphorylation.

Further examination of the active site revealed a network of interactions involving the MoO_4^{2-} or WO_4^{2-} anion and the

DOI: 10.1021/acs.biochem.5b00286
Biochemistry 2015, 54, 3514−3527

Table 3. Summary of Data Collection and Refinement Statistics for CheY·BeF_3^-·Mn^{2+} Complexes

	CheY DR·BeF_3^-·Mn^{2+}	CheY DK·BeF_3^-·Mn^{2+}	CheY DY·BeF_3^-·Mn^{2+}	CheY DQ·BeF_3^-·Mn^{2+}
		Diffraction Data		
PDB entry	3RVL	3RVP	3RVN	3RVJ
source	APS 22-BM	APS 22-ID	APS 22-BM	APS 22-BM
space group	$P2_122_1$	$P2_12_12_1$	$P2_12_12_1$	$P2_12_12_1$
a, b, c (Å)	37.63, 72.44, 107.28	53.49, 53.63, 160.42	53.44, 53.61, 161.31	53.58, 53.70, 160.66
α, β, γ (deg)	90, 90, 90	90, 90, 90	90, 90, 90	90, 90, 90
wavelength (Å)	0.97933	1.00882	0.97933	1.0
resolution (last shell) (Å)[a]	50−1.55 (1.58−1.55)	50−2.40 (2.44−2.40)	50−2.25 (2.29−2.25)	50−2.10 (2.14−2.10)
no. of unique reflections	43539	18144	22709	26982
completeness (last shell) (%)	99.3 (96.5)	96.9 (70.7)	99.8 (99.9)	96.3 (91.9)
average I/σ_I (last shell)	18.8 (3.0)	22.3 (2.6)	12.8 (2.7)	14.4 (2.4)
redundancy (last shell)	5.6 (4.0)	6.4 (3.1)	5.0 (4.4)	6.2 (4.7)
R_{sym}[b] (last shell) (%)	9.4 (40.3)	7.9 (33.7)	13.9 (53.1)	11.0 (62.4)
		Refinement		
refinement package	PHENIX 1.7_650	PHENIX 1.7_650	PHENIX 1.7_650	PHENIX 1.7_650
resolution range (Å)	25.92−1.55	44.58−2.40	27.6−2.25	27.6−2.10
no. of reflections	42133	17615	21750	26051
no. of nonsolvent atoms[c]	1930	1990	1996	1986
no. of solvent atoms and heteroatoms[c]	453	288	323	325
no. of molecules in the asymmetric unit	2	2	2	2
rmsd from ideality				
bond lengths (Å)	0.015	0.007	0.007	0.007
bond angles (deg)	1.588	1.058	1.110	1.095
R value[d] (%)	15.6	17.3	18.6	17.7
R_{free}[d] (%)	18.2	21.5	22.5	20.1

[a]Resolution limit defined as the highest-resolution shell where the average I/σ_I was >2. [b]$R_{merge} = \sum_{hkl}\sum_i|I_{i(hkl)} - \langle I_{(hkl)}\rangle|/\sum_{hkl}\sum_i I_{(hkl)}$. [c]Non-hydrogen atoms and alternate atoms are counted once. [d]$R = \sum|F_o - F_c|/\sum F_o$; ∼5% of reflections were used to calculate R_{free}.

position D + 2/T + 2 side chains. One of the key active site interactions in HAD phosphatases is the interaction between the Asp at position D + 2 and a polar residue at position T + 2, which positions the Asp appropriately for catalysis and stabilizes the active site structure.[11] In wild-type CheY, the Asn at position D + 2 is oriented away from the Glu at position T + 2 and away from the active site. A simple rotamer switch, observed in some structures of mutant CheY,[15,48] however, allows the position D + 2 Asn residue to extend toward position T + 2 and the active site. In the CheY DR·MoO_4^{2-}·Mn^{2+} and CheY DR·WO_4^{2-}·Mn^{2+} structures, the side chain of the Asp at position D + 2 assumes the rotamer directed toward the active site and forms a bidentate salt bridge with the Arg at position T + 2 (Figure 3B,C). Both the nature of the Asp (D + 2)−Arg (T + 2) interactions and the consequent positioning of the Asp at position D + 2 are highly similar to those of the interactions seen in HAD phosphatases.

The adoption of the HAD phosphatase-like positioning of the Asp at position D + 2 in CheY DR puts the side chain carboxylate within hydrogen bonding distance of the apical oxygen of the bound molybdate or tungstate anion (Figure 3B,C). Similar hydrogen bonding interactions could occur between the carboxylate side chain and the leaving group atom of a small molecule phosphodonor during phosphorylation, or an attacking water molecule during dephosphorylation, both of which would occupy nearly the same position in space as the apical oxygen atom. Thus, the orientation and novel interactions observed for positions D + 2 and T + 2 in the CheY DR cocrystal complexes with MoO_4^{2-} and WO_4^{2-} likely contribute to the accelerated autophosphorylation and autodephosphorylation rates of CheY DR.

Residues at Positions D + 2 and T + 2 Do Not Interact in the Activated Conformations of the Other CheY HAD Mimics. To assess whether the details of the active site hydrogen bonding network were unique to CheY DR, cocrystal structures of other CheY HAD mimics (CheY DQ, DY, and DK) complexed with Mn^{2+} and BeF_3^- were determined between 1.55 and 2.4 Å resolution (Table 3). In all of the cocrystal structures, the CheY backbone was quite similar to that of activated wild-type CheY (PDB entry 1FQW),[41] with Cα rmsd values of 0.263 Å for CheY DK, 0.260 Å for CheY DY, and 0.255 Å for CheY DQ. In contrast to CheY DR·MoO_4^{2-}·Mn^{2+} and CheY DR·WO_4^{2-}·Mn^{2+}, the Asp at position D + 2 is oriented away from the active site pocket and is not anchored by the polar residue at position T + 2 in CheY DQ, CheY DK, or CheY DY complexed with BeF_3^- and Mn^{2+} (Figure 4B−D). We also determined the crystal structure of CheY DR complexed with Mn^{2+} and BeF_3^-. Interestingly, the CheY DR·BeF_3^-·Mn^{2+} complex crystallized in orthorhombic space group $P2_122_1$ rather than the more common $P2_12_12_1$ space group observed previously for many BeF_3^--bound CheY cocrystal structures, likely accounting for the slightly higher rmsd (Cα rmsd of 0.633 Å) relative to wild-type CheY·BeF_3^-·Mn^{2+} (PDB entry 1FQW). With the $P2_122_1$ packing environment, the Asp at position D + 2 formed a salt bridge with Arg19 from helix α1 of a symmetry-related molecule and not with the Arg at position T + 2 within the same monomer (Figure 4F). However, the CheY DR Asp residue at position D + 2 was still oriented in the appropriate position for catalysis (Figure 4E).

Enhanced Binding of $FliM_{1-16}$ to CheY DR Indicates a More Activated Conformational Landscape. The bidendate salt bridge between the Asp at position D + 2 and the Arg at position T + 2 observed in the CheY DR·MoO_4^{2-}·Mn^{2+} and CheY DR·WO_4^{2-}·Mn^{2+} complexes, reminiscent of similar hydrogen bonding networks seen in the active sites of HAD phosphatases, raised the possibility that the CheY DR mutant had an

DOI: 10.1021/acs.biochem.5b00286
Biochemistry 2015, 54, 3514−3527

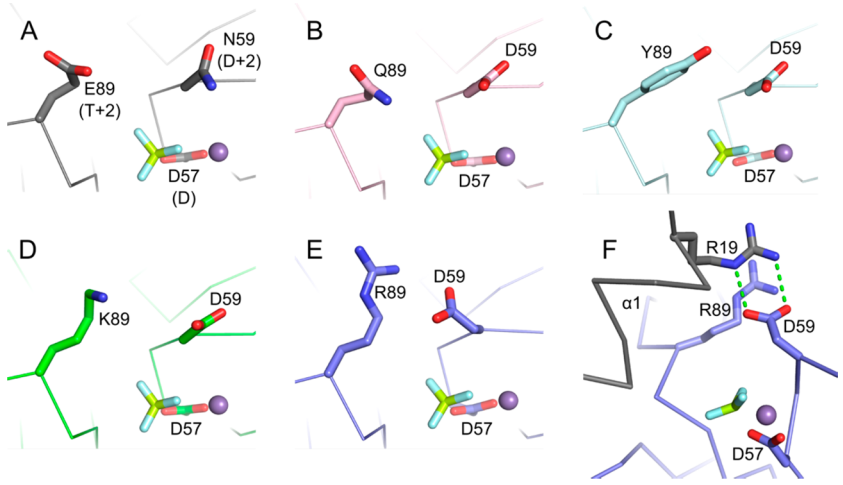

Figure 4. Positioning of residues D + 2 and T + 2 in CheYs complexed with BeF_3^- and Mn^{2+}. In wild-type CheY (A, PDB entry 1FQW), the side chain of Asn59 at position D + 2 is directed away from Glu89 at position T + 2 and is not positioned to interact with the leaving group atom (in autophosphorylation) or the nucleophilic water molecule (in autodephosphorylation). Similar orientations are observed for the Asp at position D + 2 in CheY DQ·BeF_3^-·Mn^{2+} (B, pink carbons), CheY DY·BeF_3^-·Mn^{2+} (C, cyan carbons), and CheY DK·BeF_3^-·Mn^{2+} (D, green carbons). The active site of CheY DR·BeF_3^-·Mn^{2+} (E and F, slate carbons) showed a reorientation of the Asp at position D + 2 toward the Arg at position 89 and in position to aid catalysis. The Asp at position D + 2 in the CheY DR structure does not hydrogen bond with the Arg at position T + 2 as seen in the MO_4^{2-} and WO_4^{2-} structures but instead interacts with Arg19 from helix α1 (gray) of a symmetry-related molecule (F). In all panels, BeF_3^- is shown as yellow and white sticks and M^{2+} as a purple sphere.

enhanced propensity to adopt the activated conformation. To assess this possibility, we measured binding affinities for the N-terminal peptide of the flagellar motor protein FliM ($FliM_{1-16}$) using tryptophan fluorescence[49,50] (Table 4). A

Table 4. Equilibrium Dissociation Constants for Binding of CheY to the $FliM_{1-16}$ Peptide

	amino acid		
CheY designation	position D + 2	position T + 2	K_d for $FliM_{1-16}$ (μM)[a]
	DX Set (HAD mimics)		
DR	D	R	65 ± 5
DK	D	K	120 ± 8
DY	D	Y	370 ± 30
DQ	D	Q	380 ± 50
	NX Set		
NR	N	R	180 ± 9
NK	N	K	230 ± 40
NY	N	Y	160 ± 10
wild type	N	E	370 ± 20

[a]Mean and standard deviation; n = 3.

population of CheY shifted toward a fully activated signaling conformation, by either phosphorylation or mutation, exhibits tighter binding to $FliM_{1-16}$.[49,50] $FliM_{1-16}$ binds to a CheY surface distinct from the active site, so $FliM_{1-16}$ binding affinity serves as a measure of CheY conformation that is independent of active site modification. The measured K_d for wild-type CheY (370 μM) compares reasonably to a previously published measurement from our lab (280 μM).[34] Notably, CheY DR exhibited a binding constant (K_d of 65 μM) that was nearly 6-fold tighter than that of wild-type CheY and 3-fold tighter than that of CheY NR. The K_d of 65 μM is also <3-fold weaker than reported values for $FliM_{1-16}$ binding to phosphorylated wild-type CheY (K_d = 26−27 μM),[34,49] believed to be largely in an activated conformation. The increased affinity of CheY DR for $FliM_{1-16}$ indicates that CheY DR has an enhanced propensity to acquire an activated conformation in the absence of phosphorylation. In turn, the enhanced propensity might be due to stabilization of the activated conformation of CheY DR by the interactions between the Asp at position D + 2 and the Arg at position T + 2 observed in the crystal structures.

The highly structured active site "scaffold" or "mold" of HAD phosphatases is noted as one of the contributors to their fast catalytic rates.[11] Likewise, the shift to an activated conformation could have important implications regarding the enhancement of autophosphorylation rates for CheY DR. Such models are consistent with earlier studies of the effect of switching the conformational state of CheY by binding the $FliM_{1-16}$ peptide or the P2 domain of CheA.[30] A 160-fold increase in the CheY autophosphorylation rate constant was observed for the activated versus unactivated state,[30] perhaps because of more optimal locations of conserved active site residues.[51] Thus, in addition to the positioning of the Asp at position D + 2, the enhanced autophosphorylation kinetics of CheY DR also likely have contributions from a shift toward the activated conformation. Though more modest, several of the other CheY DX and NX mutants (CheY DK, NR, NK, and NY) also exhibited binding affinities for $FliM_{1-16}$ enhanced relative to that of wild-type CheY (Table 4). Thus, shifts in relative activation also likely contribute to the enhanced PAM autophosphorylation rate constants for these CheYs (Table 1).

A shift to an activated conformation could potentially be evident from crystal structures of CheY determined in the absence of a phosphate or phosphoryl group analogue. We determined four crystal structures to investigate this possibility. However, only the unactivated conformation was observed in crystal structures of CheY DR, DK, DY, and DQ complexed with Mn^{2+} in the absence of BeF_3^- (Table S1 of the Supporting Information). This suggests that the conditions used for crystallization preferentially stabilize the unactive conformation. Furthermore, the observation of CheY DR in the unactive conformation reveals that despite more facile transitions implied by the $FliM_{1-16}$ binding data, CheY DR is still conformationally

DOI: 10.1021/acs.biochem.5b00286
Biochemistry 2015, 54, 3514−3527

dynamic and, unlike the HAD phosphatases, does not constitutively maintain a complete active site mold.

DISCUSSION

Meticulous regulation of the rates of both phosphorylation and dephosphorylation of response regulator signaling proteins is essential for effective signal transduction. Here we extend our use of CheY as a model system to elucidate mechanisms of response regulator rate modulation by assessing mechanistic similarities to a family of enzymes (HAD phosphatases) that catalyze nearly identical chemistry using a highly similar active site. Structural and biochemical characterization of a set of CheY double mutants designed to mimic the more efficient HAD phosphatases revealed that one of the engineered CheYs, CheY DR, acquired some properties of the HADs that resulted in enhanced reaction rate constants, although CheY DR appeared to fall short of bona fide acid/base catalysis or an active site preformed to fit the transition state. The results highlight the role of an active site hydrogen bonding network that allows direct interaction with the leaving group/nucleophile atom in rate enhancement of both autophosphorylation and dephosphorylation of response regulators. Additionally, the results provided insight into how the propensity to adopt the activated global conformation positively modulates response regulator catalysis.

Anchoring of the Asp at Position D + 2 by the Residue at Position T + 2 Enhances Catalysis in HAD Enzymes and CheY DR. The importance of "pinning" the Asp at position D + 2 in position to allow HAD phosphatases to function as acid/base catalysts is supported by a large body of structural and functional analysis.[11,52−54] Pinning almost exclusively occurs through hydrogen bonding interactions between the side chains of the Asp at position D + 2 and the residue at position T + 2, usually an Arg, Lys, Thr, Trp, or Tyr.[11] In the one HAD phosphatase of which we are aware that has been directly tested experimentally, substitution of the anchoring residue at position T + 2 (an arginine) results in a loss of hexose phosphate phosphatase catalytic activity similar in magnitude to that seen upon substitution of the catalytic Asp at position D + 2.[11]

Structures of CheY DR bound to the substrate/product analogues WO_4^{2-} and MO_4^{2-} revealed an active site configuration with features of a HAD phosphatase. The geometries of the bidentate salt bridge between the Asp and Arg side chains in CheY DR mimicked those of the Asp−Arg interactions in multiple HAD structures and placed the Asp at position D + 2 in the rotameric form (Figure 3B,C) to hydrogen bond with the apical oxygen atom of WO_4^{2-} or MO_4^{2-}, which occupied the space expected for the nucleophilic water oxygen or leaving group nitrogen. The unique interactions between the position D + 2 and T + 2 side chains observed in CheY DR but absent from other CheY DX variants (Figure 4) correlate with the highest rate constants for catalysis of both PAM autophosphorylation and autodephosphorylation (Table 1).

Hydrogen Bonding Interactions versus Acid/Base Catalysis as Mechanisms of Catalysis. Despite the structural evidence that correlated the anchoring of Asp at position D + 2 with enhanced catalysis, our pH profile data indicated that CheY DR was unlikely to act as a true acid/base catalyst. The rate constants for CheY DR and DY autodephosphorylation were pH-independent (Figure 2A), ruling out base catalysis. The autophosphorylation experiment for assessing acid catalysis (Figure 2B) was less direct, because the PAM phosphodonor can acquire the proton required for reaction without assistance from CheY. However, the pH dependence of the bimolecular autophosphorylation rate constant was indistinguishable for all five CheY variants tested, indicating that the Asp at position D+2 (absent from wild-type CheY) likely does not act as an acid catalyst in CheY DR. The more compelling evidence that the Asp at position D + 2 is not a base catalyst in CheY DR also implies that the Asp at position D + 2 does not act as a dual acid/base catalyst in CheY DR as it does in HAD phosphatases.

Additional evidence against acid catalysis in CheY DR can be inferred from examination of autophosphorylation with AcP. AcP does not require protonation to react with CheY, but acid catalysis would be expected to accelerate the reaction. For the Asp at position D + 2 to serve as an acid catalyst, the pK_a should be shifted to result in protonation near neutral pH. However, all of the CheY DX variants tested had rate constants for reaction with AcP substantially slower than those of their CheY NX counterparts (Table 1). Because negative charge at positions D + 2 and T + 2 retards CheY autophosphorylation with AcP,[23] we can infer that the Asp at position D + 2 is likely unprotonated. Furthermore, exploratory experiments revealed no effect of pH on autophosphorylation of CheY DR with 100 mM AcP across the pH range from 4.7 to 8.0 (data not shown), again suggesting the Asp at position D + 2 in CheY DR is not protonated and therefore does not act as an acid catalyst.

The rate enhancements of autophosphorylation with PAM and autodephosphorylation observed for CheY DR compared to those of CheY NR (Table 1) therefore must be due to effects of the oriented Asp side chain other than acid/base catalysis. For dephosphorylation, this could be positioning the water molecule for in-line nucleophilic attack. Positioning the water molecule as a mechanism to enhance response regulator dephosphorylation is the strategy used by multiple families of response regulator phosphatases. The CheX,[55] CheZ,[56] Rap,[57] and His KA_3 sensor kinase[58] families of response regulator phosphatases all function by inserting a side chain (Gln, Asn, or Thr) into the active site of the response regulator to hydrogen bond with (and position) the attacking water molecule. For autophosphorylation by PAM, direct interaction between the carboxylate oxygen on the Asp at position D + 2 and the cationic nitrogen on PAM would be expected to enhance PAM binding through positive electrostatic interactions (salt bridge formation). This stabilizing interaction would be expected to persist in the transition state where the nitrogen atom carries a partial positive charge.

The proposed introduction of hydrogen bonding interactions between the Asp at position D + 2 and nucleophilic/leaving group atoms as the mechanism of CheY DR rate enhancement (as well as the absence of acid/base catalysis) is consistent with the magnitude of reaction rate enhancements exhibited by CheY DR, which were $\sim 10^1-10^2$-fold greater than those of CheY NR or wild-type CheY (Table 1). Response regulator phosphatases, which function by positioning the water, generally provide an approximately 1−2 order of magnitude increase in the rate of dephosphorylation over that catalyzed by a response regulator in the absence of its phosphatase.[55,56] There is also evidence from HAD phosphatases that orienting hydrogen bonds increase catalytic rates $\sim 10^1-10^2$-fold.[8,59,60] In contrast, the involvement of a bona fide catalytic acid/base typically increases rates by $\sim 10^2-10^4$-fold.[61]

What structural feature(s) present in HAD phosphatases but absent in CheY DR might account for the lack of acid/base catalysis for CheY DR? One structural difference is the HAD cap domain,[8] which, when closed over the active site, yields a relatively hydrophobic pocket. This hydrophobic environment facilitates the shift in pK_a toward neutral for the catalytic Asp,

DOI: 10.1021/acs.biochem.5b00286
Biochemistry 2015, 54, 3514−3527

allowing for acid/base catalysis.[46] Even the so-called "capless" HAD phosphatases, which typically dephosphorylate macromolecular substrates, benefit from a hydrophobic active site pocket created by the HAD−substrate interface.[62,63] In contrast, CheY has a surface-exposed active site and lacks a capping domain. CheY position T + 2 mutants that increase the nonpolar surface area at the active site do enhance autophosphorylation[23] but are apparently not sufficient to functionally mimic a capping domain.

Global Conformation as a Kinetic Determinant for CheY DX. The active site for many HAD enzymes has been likened to a preformed mold where the catalytic residues are arranged similarly throughout the catalytic cycle.[11] In contrast, response regulators are allosteric proteins with activated and unactivated global conformational states that are in dynamic equilibrium.[21,41] For unphosphorylated response regulators, the equilibrium lies toward the unactive conformation. However, "pushing" the conformational equilibrium toward the activated conformation by mutation,[35] relief of inhibitory interactions with the output domain,[64] or providing a binding partner[30,65] can accelerate autophosphorylation >100-fold.[30,64] Although the mechanistic basis for the rate enhancement is not fully understood, the structure of unphosphorylated CheY bound to $FliM_{1-16}$[51] (which has many but not all of the features of a fully activated conformation) shows that the conserved Thr87 has shifted closer to the other catalytic residues and thus may provide a more complete active site mold, reminiscent of the HAD enzymes.

Our observation that unphosphorylated CheY DR exhibited enhanced binding to $FliM_{1-16}$, the peptide target of phosphorylated CheY, provided compelling evidence of a shift to a conformation that is more active for both autophosphorylation and output signaling. FliM binds to the $\beta4\alpha4$ surface on CheY, a surface distal from the active site whose topology is changed as a result of phosphorylation. The 6-fold enhancement of binding of $FliM_{1-16}$ by CheY DR ($K_d \sim 65\ \mu M$) relative to that of wild-type CheY ($K_d \sim 370\ \mu M$) is considerable compared to the ∼10−14-fold[30,49] enhancement in $FliM_{1-16}$ binding upon CheY phosphorylation. However, it is clear that CheY DR, while shifted more toward an activated conformation than wild-type CheY, is not "locked" in the activated conformation. The structure of CheY DR·Mn^{2+} (no substrate, product, or phosphoryl group analogue present) displayed an unactivated conformation. Although the backbone is in the fully activated conformation in the CheY DR complexes with MoO_4^{2-} and WO_4^{2-}, the presence of the substrate/product analogue may tip the delicate energy balance between conformational states toward the activated conformation. Though this enhancement is more modest than that of CheY DR, several of the other CheY DX and NX mutants also displayed enhanced FliM binding affinities relative to that of wild-type CheY (Table 4). Thus, these CheY mutants may also have conformational equilibria shifted toward a more activated conformation as a contribution to their enhanced autophosphorylation. For example, CheY DK and CheY NY exhibited both enhanced autophosphorylation rate constants with PAM and modestly (∼2-fold) enhanced FliM binding relative to those of wild-type CheY. It is tempting to speculate that the observed dual hydrogen bonding interactions between Asp at position D + 2 and Arg at position T + 2 (Figure 3B,C) may contribute energy to the conformational shift of CheY DR. In the absence of a substrate/product analogue, the same additional interactions could lower the energy of the activated conformation. Conformation is expected to have a weaker impact on the control of autodephosphorylation rates for response regulators because the reactant (CheY−P) is already in an activated conformation.

Structural Relationships between Response Regulators and HAD Enzymes. The hallmarks of the CheY DR·MoO_4^{2-} and CheY DR·WO_4^{2-} structures presented here were that (1) the CheY backbone was in the fully activated conformation and (2) the activated conformation allowed interactions between conserved active site features and MoO_4^{2-} or WO_4^{2-} that directly mimicked those seen with HAD complexes. Together, these properties provide direct evidence of the notion that the nature of the protein·substrate or protein·product complexes in response regulators is highly similar to that of HAD phosphatases.

Structures of HAD phosphatases containing a phosphate or a phosphate analogue in the active site have served as informative models of enzyme·substrate complexes (e.g., ref 16), and it is notable that such structures constitute a significant fraction of the total HAD structures in current public databases. In our survey of 285 HAD structures (compiled from PDB searches for Pfam groups PF00702, PF03767, PF12689, and PF08645), we found 71 that contained inorganic phosphate, a phosphate analogue, or a phosphate-containing substrate properly oriented in the HAD active site mold. In each of these structures, the HAD phosphate analogue structures show conserved interactions between three phosphate oxygen atoms (or equivalent) and the bound divalent metal ion, the conserved Thr, and Lys. These interactions are preserved in structures of many of the same HAD phosphatases complexed with planar molecules that model the transition state and thus are likely to stay intact throughout the reaction cycle.

In contrast, in a survey of 255 receiver domain structures (excluding the structures presented in this report), we identified only seven PDB entries (four different response regulators) with a HPO_4^{2-} (phosphate) or HPO_4^{2-} analogue within the active site, even though many of the structures were determined using crystals containing high concentrations of SO_4^{2-}, a phosphate analogue. Strikingly, in all seven of these structures (PDB entries 3GWG, 3H1G, 3H1F, 3OO0, 3DGE, 1I3C, and 1JLK),[66−68] like the CheY DR·MoO_4^{2-} and CheY DR·WO_4^{2-} structures reported here, the receiver domain was in an activated global conformation. Of the seven entries, four also contained a divalent metal ion, and in three of these four (PDB entries 3GWG, 3H1G, and 3OO0), there are direct interactions between the oxygen atoms of the phosphoryl analogue (sulfate in all cases) and the M^{2+}, Lys, and Thr, as observed in HAD phosphatase·substrate structures. To the best of our knowledge, no response regulator structures have been determined with an actual small molecule substrate bound to the active site. The paucity of structures for response regulators with a bound active site phosphate/phosphate analogue is likely caused by the fact that unphosphorylated response regulators are dominated by the unactivated conformation and only very weakly bind phosphate. In the same vein, the correlation between the presence of the activated conformation and a bound phosphate/phosphate analogue is consistent with the notion that the activated conformation of response regulators is the reactive molecule for phosphorylation[26,30,64,65] and, further, that the interactions between active site residues and substrate/product molecules are highly similar to those in HAD phosphatases. Response regulator proteins such as CheY DR that form crystallizable complexes with phosphate analogues may serve as good candidates for which to attempt cocrystallization with substrate analogues or planar transition state analogues, as has already been achieved for multiple HAD phosphatases.

Enzyme Families with Functionally Tuned Reaction Mechanisms. Receiver domains and HAD enzymes are

DOI: 10.1021/acs.biochem.5b00286
Biochemistry 2015, 54, 3514−3527

distantly related and share structural similarities.[69] However, the reactions catalyzed by receiver domains and HAD phosphatases have diverged kinetically to fulfill different purposes. HAD phosphatases, with the conserved Asp at position D + 2 providing acid/base catalysis, the anchoring residue at position T + 2, and a structured active site, support rapid hydrolysis of the phosphoryl group both from the substrate and from the phospho-enzyme intermediate. Receiver domains, lacking the catalytic Asp at position D + 2 and undergoing allosteric conformational changes, support a relatively stable phospho-enzyme intermediate for signal transduction. Our attempt to endow a receiver domain with HAD-like properties by engineering specific residues at positions D + 2 and T + 2 was partially successful.

A potentially analogous circumstance is provided by the GHKL protein superfamily, composed of gyrase-like topoisomerases, Hsp90 chaperones, histidine kinases, and MutL DNA repair enzymes.[70] Each constituent family contains a similar ATP binding domain, which supports ATP hydrolysis in three (gyrases, Hsp90s, and MutLs) of the four families. In each case, ATP hydrolysis is coupled to protein conformational changes associated with interactions with their macromolecular substrates.[71,72] In contrast, in histidine kinases, the γ-phosphoryl group of ATP is transferred to a His residue instead of water. The phospho-His residue then fulfills a signal transduction function, serving as the phosphodonor for receiver domains. The absence of ATPase activity in the histidine kinases is hypothesized to be due to lack of a conserved Glu that serves as a catalytic base, as well as lack of a positively charged Lys or Arg that interacts with the γ-phosphoryl group of ATP.[70,73,74] Nevertheless, GHKL ATP binding domains are sufficiently similar that radicicol, a drug that inhibits the ATPase activities of Hsp90s and topoisomerases,[75] also inhibits the autophosphorylation activity of at least two histidine kinases.[76,77]

To the best of our knowledge, restoration of ATPase activity in histidine kinases by introduction of the catalytic Glu found in GHL family members has not been attempted. However, engineering a monovalent cation binding site from a K family member into a GHL protein has been achieved.[78] When an Ala adjacent to the MutL cation binding site was replaced with a Pro found in kinases, the coordination of the ion in MutL changed (two ligands lost and two gained) to display the same coordination found in the kinase that inspired the Pro substitution. However, the binding site in the kinase is specific for potassium, whereas the mutant MutL binding site with the same coordination pattern is specific for sodium. As with our attempt to engineer HAD phosphatase properties into a receiver domain, transplanting a key amino acid onto a related protein backbone endowed the recipient with some, but not all, of the properties of the "donor" protein.

■ ASSOCIATED CONTENT

Supporting Information

A summary of data collection and refinement statistics for CheY DR·Mn^{2+}, CheY DK·Mn^{2+}, CheY DY·Mn^{2+}, and CheY DQ·Mn^{2+} (Table S1) and electron density maps in the active site regions of CheY DR complexed with Mn^{2+} and MoO_4^{2-} or WO_4^{2-} (Figure S1). The Supporting Information is available free of charge on the ACS Publications website at DOI: 10.1021/acs.biochem.5b00286.

Accession Codes

Coordinates from the X-ray structures were deposited in the Protein Data Bank as entries 3RVJ, 3RVK, 3RVL, 3RVM, 3RVN, 3RVO, 3RVP, 3RVQ, 3RVR, and 3RVS.

■ AUTHOR INFORMATION

Corresponding Author

*Department of Microbiology and Immunology, University of North Carolina, Chapel Hill, NC 27599-7290. E-mail: bourret@med.unc.edu. Telephone: (919) 966-2679. Fax: (919) 962-8103.

Present Address

†C.A.S.: Department of Pharmacology, Vanderbilt University, 460 Robinson Research Building, 2220 Pierce Ave., Nashville, TN 37232-6600.

Funding

This work was supported by National Institutes of Health Grant R01GM050860 awarded to R.B.B. C.S. was supported by National Institutes of Health Grant R25 GM089569. Financial support for use of beamlines 22-BM and 22-ID at the Advanced Photon Source (Argonne National Laboratory, Argonne, IL) was supported by the U.S. Department of Energy, Office of Science, Office of Basic Energy Sciences, under Contract W-31-109-Eng-3 and the Southeast Regional Collaborative Access Team (SER-CAT).

Notes

The authors declare no competing financial interest.

■ ACKNOWLEDGMENTS

We thank Karen Allen for very helpful discussions about HAD enzymes and Ash Tripathy at the Macromolecular Interaction Facility at the University of North Carolina for help with stopped-flow fluorescence measurements.

■ ABBREVIATIONS

D, conserved phosphorylated aspartate shared by response regulators and HAD phosphatases; T, conserved threonine/serine shared by response regulators and HAD phosphatases; K, conserved lysine shared by response regulators and HAD phosphatases; DD, conserved acid residues that coordinate the Mg^{2+} shared by response regulators and HAD phosphatases; D + 2 and T + 2, position in the primary sequence of response regulators or HAD phosphatases that is two residues carboxyl-terminal to D and T, respectively; CheY DX, *E. coli* CheY double mutant with an Asp substituted for Asn59 at position D + 2 and X representing the residue substituted for Glu89 at position T + 2; AcP, acetyl phosphate; PAM, phosphoramidate; PDB, Protein Data Bank.

■ REFERENCES

(1) Bourret, R. B., and Silversmith, R. E. (2010) Two-component signal transduction. *Curr. Opin. Microbiol. 13*, 113−115.

(2) Capra, E. J., and Laub, M. T. (2012) Evolution of two-component signal transduction systems. *Annu. Rev. Microbiol. 66*, 325−347.

(3) Lukat, G. S., McCleary, W. R., Stock, A. M., and Stock, J. B. (1992) Phosphorylation of bacterial response regulator proteins by low molecular weight phospho-donors. *Proc. Natl. Acad. Sci. U.S.A. 89*, 718−722.

(4) Silversmith, R. E., Appleby, J. L., and Bourret, R. B. (1997) Catalytic mechanism of phosphorylation and dephosphorylation of CheY: Kinetic characterization of imidazole phosphates as phosphodonors and the role of acid catalysis. *Biochemistry 36*, 14965−14974.

(5) Hess, J. F., Bourret, R. B., Oosawa, K., Matsumura, P., and Simon, M. I. (1988) Protein phosphorylation and bacterial chemotaxis. *Cold Spring Harbor Symp. Quant. Biol. 53* (Part 1), 41−48.

(6) Wolanin, P. M., Webre, D. J., and Stock, J. B. (2003) Mechanism of phosphatase activity in the chemotaxis response regulator CheY. *Biochemistry 42*, 14075−14082.

(7) Cho, H., Wang, W., Kim, R., Yokota, H., Damo, S., Kim, S. H., Wemmer, D., Kustu, S., and Yan, D. (2001) BeF_3^- acts as a phosphate

DOI: 10.1021/acs.biochem.5b00286
Biochemistry 2015, 54, 3514−3527

analog in proteins phosphorylated on aspartate: Structure of a BeF_3^- complex with phosphoserine phosphatase. *Proc. Natl. Acad. Sci. U.S.A. 98*, 8525−8530.
(8) Allen, K. N., and Dunaway-Mariano, D. (2004) Phosphoryl group transfer: Evolution of a catalytic scaffold. *Trends Biochem. Sci. 29*, 495−503.
(9) Lu, Z., Dunaway-Mariano, D., and Allen, K. N. (2005) HAD superfamily phosphotransferase substrate diversification: Structure and function analysis of HAD subclass IIB sugar phosphatase BT4131. *Biochemistry 44*, 8684−8696.
(10) Ridder, I. S., and Dijkstra, B. W. (1999) Identification of the Mg^{2+}-binding site in the P-type ATPase and phosphatase members of the HAD (haloacid dehalogenase) superfamily by structural similarity to the response regulator protein CheY. *Biochem. J. 339* (Part 2), 223−226.
(11) Lu, Z., Dunaway-Mariano, D., and Allen, K. N. (2008) The catalytic scaffold of the haloalkanoic acid dehalogenase enzyme superfamily acts as a mold for the trigonal bipyramidal transition state. *Proc. Natl. Acad. Sci. U.S.A. 105*, 5687−5692.
(12) Collet, J. F., Stroobant, V., and Van Schaftingen, E. (1999) Mechanistic studies of phosphoserine phosphatase, an enzyme related to P-type ATPases. *J. Biol. Chem. 274*, 33985−33990.
(13) Seifried, A., Schultz, J., and Gohla, A. (2012) Human HAD phosphatases: Structure, mechanism, and roles in health and disease. *FEBS J. 280*, 549−571.
(14) Kuznetsova, E., Proudfoot, M., Gonzalez, C. F., Brown, G., Omelchenko, M. V., Borozan, I., Carmel, L., Wolf, Y. I., Mori, H., Savchenko, A. V., Arrowsmith, C. H., Koonin, E. V., Edwards, A. M., and Yakunin, A. F. (2006) Genome-wide analysis of substrate specificities of the *Escherichia coli* haloacid dehalogenase-like phosphatase family. *J. Biol. Chem. 281*, 36149−36161.
(15) Pazy, Y., Wollish, A. C., Thomas, S. A., Miller, P. J., Collins, E. J., Bourret, R. B., and Silversmith, R. E. (2009) Matching biochemical reaction kinetics to the timescales of life: Structural determinants that influence the autodephosphorylation rate of response regulator proteins. *J. Mol. Biol. 392*, 1205−1220.
(16) Wang, W., Cho, H. S., Kim, R., Jancarik, J., Yokota, H., Nguyen, H. H., Grigoriev, I. V., Wemmer, D. E., and Kim, S. H. (2002) Structural characterization of the reaction pathway in phosphoserine phosphatase: Crystallographic "snapshots" of intermediate states. *J. Mol. Biol. 319*, 421−431.
(17) Dai, J., Finci, L., Zhang, C., Lahiri, S., Zhang, G., Peisach, E., Allen, K. N., and Dunaway-Mariano, D. (2009) Analysis of the structural determinants underlying discrimination between substrate and solvent in β-phosphoglucomutase catalysis. *Biochemistry 48*, 1984−1995.
(18) Zhang, M., Liu, J., Kim, Y., Dixon, J. E., Pfaff, S. L., Gill, G. N., Noel, J. P., and Zhang, Y. (2010) Structural and functional analysis of the phosphoryl transfer reaction mediated by the human small C-terminal domain phosphatase, Scp1. *Protein Sci. 19*, 974−986.
(19) Ulrich, L. E., and Zhulin, I. B. (2010) The MiST2 database: A comprehensive genomics resource on microbial signal transduction. *Nucleic Acids Res. 38*, D401−D407.
(20) Cho, H. S., Lee, S. Y., Yan, D., Pan, X., Parkinson, J. S., Kustu, S., Wemmer, D. E., and Pelton, J. G. (2000) NMR structure of activated CheY. *J. Mol. Biol. 297*, 543−551.
(21) McDonald, L. R., Boyer, J. A., and Lee, A. L. (2012) Segmental motions, not a two-state concerted switch, underlie allostery in CheY. *Structure 20*, 1363−1373.
(22) Thomas, S. A., Brewster, J. A., and Bourret, R. B. (2008) Two variable active site residues modulate response regulator phosphoryl group stability. *Mol. Microbiol. 69*, 453−465.
(23) Thomas, S. A., Immormino, R. M., Bourret, R. B., and Silversmith, R. E. (2013) Nonconserved active site residues modulate CheY autophosphorylation kinetics and phosphodonor preference. *Biochemistry 52*, 2262−2273.
(24) Gouet, P., Fabry, B., Guillet, V., Birck, C., Mourey, L., Kahn, D., and Samama, J. P. (1999) Structural transitions in the FixJ receiver domain. *Structure 7*, 1517−1526.
(25) Formaneck, M. S., Ma, L., and Cui, Q. (2006) Reconciling the "old" and "new" views of protein allostery: A molecular simulation study of chemotaxis Y protein (CheY). *Proteins 63*, 846−867.
(26) Creager-Allen, R. L., Silversmith, R. E., and Bourret, R. B. (2013) A link between autophosphorylation and dimerization of the PhoB response regulator. *J. Biol. Chem. 288*, 21755−21769.
(27) Bourret, R. B., Thomas, S. A., Page, S. C., Creager-Allen, R. L., Moore, A. M., and Silversmith, R. E. (2010) Measurement of response regulator autodephosphorylation rates spanning six orders of magnitude. *Methods Enzymol. 471*, 89−114.
(28) Hess, J. F., Bourret, R. B., and Simon, M. I. (1991) Phosphorylation assays for proteins of the two-component regulatory system controlling chemotaxis in *Escherichia coli*. *Methods Enzymol. 200*, 188−204.
(29) Boesch, K. C., Silversmith, R. E., and Bourret, R. B. (2000) Isolation and characterization of nonchemotactic CheZ mutants of *Escherichia coli*. *J. Bacteriol. 182*, 3544−3552.
(30) Schuster, M., Silversmith, R. E., and Bourret, R. B. (2001) Conformational coupling in the chemotaxis response regulator CheY. *Proc. Natl. Acad. Sci. U.S.A. 98*, 6003−6008.
(31) Da Re, S. S., Deville-Bonne, D., Tolstykh, T., Veron, M., and Stock, J. B. (1999) Kinetics of CheY phosphorylation by small molecule phosphodonors. *FEBS Lett. 457*, 323−326.
(32) Mayover, T. L., Halkides, C. J., and Stewart, R. C. (1999) Kinetic characterization of CheY phosphorylation reactions: Comparison of P-CheA and small-molecule phosphodonors. *Biochemistry 38*, 2259−2271.
(33) Roberts, A., Lee, S. Y., McCullagh, E., Silversmith, R. E., and Wemmer, D. E. (2005) YbiV from *Escherichia coli* K12 is a HAD phosphatase. *Proteins 58*, 790−801.
(34) Schuster, M., Zhao, R., Bourret, R. B., and Collins, E. J. (2000) Correlated switch binding and signaling in bacterial chemotaxis. *J. Biol. Chem. 275*, 19752−19758.
(35) Smith, J. G., Latiolais, J. A., Guanga, G. P., Pennington, J. D., Silversmith, R. E., and Bourret, R. B. (2004) A search for amino acid substitutions that universally activate response regulators. *Mol. Microbiol. 51*, 887−901.
(36) Volz, K., Beman, J., and Matsumura, P. (1986) Crystallization and preliminary characterization of CheY, a chemotaxis control protein from *Escherichia coli*. *J. Biol. Chem. 261*, 4723−4725.
(37) Zhu, X., Rebello, J., Matsumura, P., and Volz, K. (1997) Crystal structures of CheY mutants Y106W and T87I/Y106W. CheY activation correlates with movement of residue 106. *J. Biol. Chem. 272*, 5000−5006.
(38) Otwinowski, Z., and Minor, W. (1997) Processing of X-ray diffraction data collected in oscillation mode. *Methods Enzymol. 276*, 307−326.
(39) Kabsch, W. (2010) XDS. *Acta Crystallogr. D66*, 125−132.
(40) Brennan, S., and Cowan, P. L. (1992) A suite of programs for calculating X-ray absorption, reflection, and diffraction performance for a variety of materials at arbitrary wavelengths. *Rev. Sci. Instrum. 63*, 850−853.
(41) Lee, S. Y., Cho, H. S., Pelton, J. G., Yan, D., Berry, E. A., and Wemmer, D. E. (2001) Crystal structure of activated CheY. Comparison with other activated receiver domains. *J. Biol. Chem. 276*, 16425−16431.
(42) Volz, K., and Matsumura, P. (1991) Crystal structure of *Escherichia coli* CheY refined at 1.7-Å resolution. *J. Biol. Chem. 266*, 15511−15119.
(43) Emsley, P., and Cowtan, K. (2004) Coot: Model-building tools for molecular graphics. *Acta Crystallogr. D60*, 2126−2132.
(44) Adams, P. D., Afonine, P. V., Bunkoczi, G., Chen, V. B., Davis, I. W., Echols, N., Headd, J. J., Hung, L.-W., Kapral, G. J., Grosse-Kunstleve, R. W., McCoy, A. J., Moriarty, N. W., Oeffner, R., Read, R. J., Richardson, D. C., Richardson, J. S., Terwilliger, T. C., and Zwart, P. H. (2010) PHENIX: A comprehensive Python-based system for macromolecular structure solution. *Acta Crystallogr. D66*, 213−221.
(45) Chen, V. B., Arendall, W. B., III, Headd, J. J., Keedy, D. A., Immormino, R. M., Kapral, G. J., Murray, L. W., Richardson, J. S., and Richardson, D. C. (2010) MolProbity: All-atom structure validation for macromolecular crystallography. *Acta Crystallogr. D66*, 12−21.

DOI: 10.1021/acs.biochem.5b00286
Biochemistry 2015, 54, 3514−3527

(46) Harris, T. K., and Turner, G. J. (2002) Structural basis of perturbed pK_a values of catalytic groups in enzyme active sites. *IUBMB Life 53*, 85−98.
(47) Perrin, D. D. (1982) *Ionization Constants of Inorganic Acids and Bases in Aqueous Solution*, 2nd ed., Pergamon Press, Oxford, U.K.
(48) Silversmith, R. E., Guanga, G. P., Betts, L., Chu, C., Zhao, R., and Bourret, R. B. (2003) CheZ-mediated dephosphorylation of the *Escherichia coli* chemotaxis response regulator CheY: Role for CheY glutamate 89. *J. Bacteriol. 185*, 1495−1502.
(49) McEvoy, M. M., Bren, A., Eisenbach, M., and Dahlquist, F. W. (1999) Identification of the binding interfaces on CheY for two of its targets, the phosphatase CheZ and the flagellar switch protein, FliM. *J. Mol. Biol. 289*, 1423−1433.
(50) Shukla, D., Zhu, X. Y., and Matsumura, P. (1998) Flagellar motor-switch binding face of CheY and the biochemical basis of suppression by CheY mutants that compensate for motor-switch defects in *Escherichia coli*. *J. Biol. Chem. 273*, 23993−23999.
(51) Dyer, C. M., and Dahlquist, F. W. (2006) Switched or not?: The structure of unphosphorylated CheY bound to the N terminus of FliM. *J. Bacteriol. 188*, 7354−7363.
(52) Zhang, G., Dai, J., Wang, L., Dunaway-Mariano, D., Tremblay, L. W., and Allen, K. N. (2005) Catalytic cycling in β-phosphoglucomutase: A kinetic and structural analysis. *Biochemistry 44*, 9404−9416.
(53) Nguyen, H. H., Wang, L., Huang, H., Peisach, E., Dunaway-Mariano, D., and Allen, K. N. (2010) Structural determinants of substrate recognition in the HAD superfamily member D-glycero-D-manno-heptose-1,7-bisphosphate phosphatase (GmhB). *Biochemistry 49*, 1082−1092.
(54) Lahiri, S. D., Zhang, G., Dunaway-Mariano, D., and Allen, K. N. (2002) Caught in the act: The structure of phosphorylated β-phosphoglucomutase from *Lactococcus lactis*. *Biochemistry 41*, 8351−8359.
(55) Pazy, Y., Motaleb, M. A., Guarnieri, M. T., Charon, N. W., Zhao, R., and Silversmith, R. E. (2010) Identical phosphatase mechanisms achieved through distinct modes of binding phosphoprotein substrate. *Proc. Natl. Acad. Sci. U.S.A. 107*, 1924−1929.
(56) Zhao, R., Collins, E. J., Bourret, R. B., and Silversmith, R. E. (2002) Structure and catalytic mechanism of the *E. coli* chemotaxis phosphatase CheZ. *Nat. Struct. Biol. 9*, 570−575.
(57) Parashar, V., Mirouze, N., Dubnau, D. A., and Neiditch, M. B. (2011) Structural basis of response regulator dephosphorylation by Rap phosphatases. *PLoS Biol. 9*, e1000589.
(58) Huynh, T. N., Noriega, C. E., and Stewart, V. (2010) Conserved mechanism for sensor phosphatase control of two-component signaling revealed in the nitrate sensor NarX. *Proc. Natl. Acad. Sci. U.S.A. 107*, 21140−21145.
(59) Sorensen, T. L., Dupont, Y., Vilsen, B., and Andersen, J. P. (2000) Fast kinetic analysis of conformational changes in mutants of the Ca^{2+}-ATPase of sarcoplasmic reticulum. *J. Biol. Chem. 275*, 5400−5408.
(60) Clausen, J. D., McIntosh, D. B., Woolley, D. G., and Andersen, J. P. (2001) Importance of Thr-353 of the conserved phosphorylation loop of the sarcoplasmic reticulum Ca^{2+}-ATPase in MgATP binding and catalytic activity. *J. Biol. Chem. 276*, 35741−35750.
(61) Fersht, A. (1999) *Structure and Mechanism in Protein Science*, W. H. Freeman and Co., New York.
(62) Peisach, E., Wang, L., Burroughs, A. M., Aravind, L., Dunaway-Mariano, D., and Allen, K. N. (2008) The X-ray crystallographic structure and activity analysis of a *Pseudomonas*-specific subfamily of the HAD enzyme superfamily evidences a novel biochemical function. *Proteins 70*, 197−207.
(63) Galburt, E. A., Pelletier, J., Wilson, G., and Stoddard, B. L. (2002) Structure of a tRNA repair enzyme and molecular biology workhorse: T4 polynucleotide kinase. *Structure 10*, 1249−1260.
(64) Barbieri, C. M., Mack, T. R., Robinson, V. L., Miller, M. T., and Stock, A. M. (2010) Regulation of response regulator autophosphorylation through interdomain contacts. *J. Biol. Chem. 285*, 32325−32335.
(65) Ames, S. K., Frankema, N., and Kenney, L. J. (1999) C-terminal DNA binding stimulates N-terminal phosphorylation of the outer membrane protein regulator OmpR from *Escherichia coli*. *Proc. Natl. Acad. Sci. U.S.A. 96*, 11792−11797.
(66) Casino, P., Rubio, V., and Marina, A. (2009) Structural insight into partner specificity and phosphoryl transfer in two-component signal transduction. *Cell 139*, 325−336.
(67) Im, Y. J., Rho, S. H., Park, C. M., Yang, S. S., Kang, J. G., Lee, J. Y., Song, P. S., and Eom, S. H. (2002) Crystal structure of a cyanobacterial phytochrome response regulator. *Protein Sci. 11*, 614−624.
(68) Lam, K. H., Ling, T. K., and Au, S. W. (2010) Crystal structure of activated CheY1 from *Helicobacter pylori*. *J. Bacteriol. 192*, 2324−2334.
(69) Burroughs, A. M., Allen, K. N., Dunaway-Mariano, D., and Aravind, L. (2006) Evolutionary genomics of the HAD superfamily: Understanding the structural adaptations and catalytic diversity in a superfamily of phosphoesterases and allied enzymes. *J. Mol. Biol. 361*, 1003−1034.
(70) Dutta, R., and Inouye, M. (2000) GHKL, an emergent ATPase/kinase superfamily. *Trends Biochem. Sci. 25*, 24−28.
(71) Corbett, K. D., and Berger, J. M. (2005) Structural dissection of ATP turnover in the prototypical GHL ATPase TopoVI. *Structure 13*, 873−882.
(72) Pearl, L. H., and Prodromou, C. (2006) Structure and mechanism of the Hsp90 molecular chaperone machinery. *Annu. Rev. Biochem. 75*, 271−294.
(73) Cunningham, C. N., Southworth, D. R., Krukenberg, K. A., and Agard, D. A. (2012) The conserved arginine 380 of Hsp90 is not a catalytic residue, but stabilizes the closed conformation required for ATP hydrolysis. *Protein Sci. 21*, 1162−1171.
(74) Wilke, K. E., and Carlson, E. E. (2013) All signals lost. *Sci. Transl. Med. 5*, 203−212.
(75) Corbett, K. D., and Berger, J. M. (2006) Structural basis for topoisomerase VI inhibition by the anti-Hsp90 drug radicicol. *Nucleic Acids Res. 34*, 4269−4277.
(76) Besant, P. G., Lasker, M. V., Bui, C. D., and Turck, C. W. (2002) Inhibition of branched-chain α-keto acid dehydrogenase kinase and Sln1 yeast histidine kinase by the antifungal antibiotic radicicol. *Mol. Pharmacol. 62*, 289−296.
(77) Guarnieri, M. T., Zhang, L., Shen, J., and Zhao, R. (2008) The Hsp90 inhibitor radicicol interacts with the ATP-binding pocket of bacterial sensor kinase PhoQ. *J. Mol. Biol. 379*, 82−93.
(78) Hu, X., Machius, M., and Yang, W. (2003) Monovalent cation dependence and preference of GHKL ATPases and kinases. *FEBS Lett. 544*, 268−273.
(79) Silversmith, R. E., Smith, J. G., Guanga, G. P., Les, J. T., and Bourret, R. B. (2001) Alteration of a nonconserved active site residue in the chemotaxis response regulator CheY affects phosphorylation and interaction with CheZ. *J. Biol. Chem. 276*, 18478−18484.

DOI: 10.1021/acs.biochem.5b00286
Biochemistry 2015, 54, 3514−3527